

The threshold displacement energy of buckminsterfullerene C_{60} and formation of the endohedral defect fullerene $He@C_{59}$

Mark H. Stockett^{a,*}, Michael Wolf^a, Michael Gatchell^{a,b}, Henning T. Schmidt^a, Henning Zettergren^a, Henrik Cederquist^a

^a*Department of Physics, Stockholm University, Roslagstullsbacken 21, SE-106 91 Stockholm, Sweden*

^b*Institut für Ionenphysik und Angewandte Physik, Universität Innsbruck, Technikerstr. 25, A-6020 Innsbruck, Austria*

Abstract

We have measured the threshold center-of-mass kinetic energy for knocking out a single carbon atom from C_{60}^- in collisions with He. Combining this experimental result with classical molecular dynamics simulations, we determine a semi-empirical value of 24.1 ± 0.5 eV for the threshold displacement energy, the energy needed to remove a single carbon atom from the C_{60} cage. We report the first observation of an endohedral complex with an odd number of carbon atoms, $He@C_{59}^-$, and discuss its formation and decay mechanisms.

1. Introduction

Irradiation by electrons, ions, or atoms may displace individual atoms from their original positions in solids [1], small aggregates of matter [2], or free molecules [3]. Such defects can for example be used to tailor nanostructured materials with new intriguing functionalities [4, 5, 6], and serve as reactive sites for efficient molecular growth processes inside molecular clusters [2, 7, 8], for example in different planetary atmospheres. Introductions of defects may also be a limiting factor in high-resolution transmission electron microscopy, as material modifications during image capture may yield images that do not represent the original sample material [9, 10]. In addition, collisions with H and He atoms leading to atom displacement are thought to be important mechanisms for destruction of large molecules in the interstellar medium [11, 12]. The key intrinsic (projectile independent) target property quantifying the effect of these types of radiation damage is the so-called threshold displacement energy, T_d , the minimum energy transfer to a single atom required to permanently displace it from its initial position [1].

The threshold displacement energy is distinct from related quantities such as the dissociation energy or the vacancy energy in that it includes the energy barrier between the parent and product states. While independent of projectile, T_d depends somewhat on the angle between the momentum imparted to the primary knock-on atom and the inter-atomic bonds [13, 14]. Nevertheless, typical values of T_d are widely used to model radiation damage across wide ranges of energy. In recent breakthrough experiments [15, 16], the threshold displacement energy for single-layer

graphene was reported to be $T_d = 23.6$ eV. Similar values for T_d have also been deduced for gas-phase Polycyclic Aromatic Hydrocarbon (PAH) molecules [17].

Here, we determine the $C_{60} \rightarrow C_{59} + C$ threshold displacement energy for isolated C_{60} , which has a perfectly symmetric icosahedral structure where the C atoms have a different hybridization than graphene or PAHs. With all atoms equivalent, C_{60} is the ideal prototype for displacement studies of molecules. Previously reported values of T_d for C_{60} from electron microscopy experiments and from Molecular Dynamics simulations have spanned a wide range from 7.6–15.7 eV [18] and 29.1 eV [13], respectively. Models of radiation damage to fullerenes have generally assumed a value in the middle of this range, around 15 eV, equivalent to the vacancy energy [19, 20, 2].

In addition to the threshold displacement energy for C_{60} , we also report the first observation of the endohedral defect fullerene complex $He@C_{59}^-$ formed in collisions where the He is captured following C displacement. Endohedral complexes $B@C_{2n}$, where an atom or molecule B is trapped inside the fullerene cage, has been of interest since the dawn of the fullerene era, both from pure and applied perspectives [21, 22, 23, 24, 25]. The present observation of $He@C_{59}^-$ provides insight into the formation and stability of endohedral complexes with odd numbers of carbon atoms.

In typical fullerene fragmentation experiments, energy deposited through interactions with *e.g.* photons, electrons, or fast ions is converted into internal vibrational energy. For C_{60} , where $C_{60} \rightarrow C_{58} + C_2$ is the lowest energy dissociation channel [26, 27], this leads to the well-known statistical product distribution dominated by fragments with even numbers of carbon atoms, C_{60-2n} , $n = 1, 2, \dots$. In collision experiments like those presented here, products with odd numbers of C atoms like C_{59} have occasionally

*Corresponding author

Email address: Mark.Stockett@fysik.su.se
(Mark H. Stockett)

been observed [21, 20, 26, 28]. These products are fingerprints of non-statistical fragmentation, where carbon atoms are displaced in billiard-ball like collisions [3]. This process takes place on timescales that are too short (sub-femtoseconds) for local excitations to distribute over the whole molecular system. The exceptionally low yield of C_{59}^- relative to statistical fragmentation products has so far precluded systematic experimental studies of this mechanism.

Here, we have developed a refined approach to determine displacement energies for free molecules in collisions with particles that improves upon earlier such methods in an important way, namely by eliminating the (usually dominant) contribution of statistical fragmentation from the product distribution. This is achieved by colliding He with C_{60}^- ions and measuring the threshold behavior for the formation of *negatively charged* fragments *e.g.* C_{59}^- and C_{58}^- . Because the electron affinity of C_{60} (2.664 eV [29]) is much lower than any of the dissociation energies of the system (which are > 10 eV [26, 27], see also Tables 1 and 2 below), any trajectories depositing enough energy to induce statistical unimolecular dissociation most likely lead to electron loss and thus do not contribute to the negative ion product spectrum. In this way, we select those trajectories where essentially all the excitation energy is transferred to the primary knock-on atom, and as little as possible to the other atoms in the C_{60} cage or to the electronic degrees of freedom. By eliminating the major source of background from the measurement, greater sensitivity to minute cross-sections for non-statistical fragmentation is achieved, without which the present results for C_{60} would not be possible. We combine experimental measurements of the threshold center-of-mass energy for non-statistical fragmentation of C_{60}^- in collisions with He with classical Molecular Dynamics (MD) simulations of the knockout process and a statistical model of electron loss from C_{60}^- and C_{59}^- to determine the threshold displacement energy T_d . Because the extra electron in C_{60}^- has only a small effect on the binding between C atoms, this result applies to neutral as well as anionic C_{60} .

2. Methods

2.1. Experiments

Experiments were performed using the Electrospray Ion Source Laboratory (EISLAB) accelerator mass spectrometer, which has been described previously [30, 31]. Continuous beams of C_{60}^- were produced by means of ElectroSpray Ionization, with tetrathiafulvalene (TTF) added as an electron donor [32] to a 1:1 mixture of methanol and dichloromethane containing fullerite. In the ion source, the C_{60}^- ions undergo many low-energy collisions and are assumed to equilibrate to roughly room temperature. Following production of the ions by ESI, an ion funnel was used to collect and focus the ions. Two octupole ion

guides transported the ions through two stages of differential pumping. A quadrupole mass filter was used to mass-select C_{60}^- ions, which were then accelerated to 3–15 keV and passed through a 4 cm long collision cell containing the target gas (He). This C_{60}^- kinetic energy range corresponds to center-of-mass energies, E_{CM} , of 20–80 eV for collisions with He in the cell. An Einzel lens and two pairs of electrostatic deflector plates served as a large-angular-acceptance kinetic-energy-per-charge analyzer after the gas cell. Intact C_{60}^- and daughter anions were detected on a 40 mm multi-channel plate (MCP) with a position-sensitive resistive anode. The deflection voltage combined with the position on the MCP (along the direction of deflection) of each detected anion was used to calculate its kinetic energy per charge [31].

Total destruction cross sections (*i.e.* the sum of the cross sections for all processes – fragmentation and/or electron-loss or ionization processes – that change the mass-to-charge ratio of C_{60}^- in collisions with He under the present experimental conditions) were determined by measuring the attenuation of the parent C_{60}^- beam as a function of target gas density. The attenuation is fit to a single exponential decay

$$\Gamma(p) = \Gamma_0 e^{-p\sigma l/k_B T} \quad (1)$$

where $\Gamma(p)$ is the parent C_{60}^- count rate as a function of the He pressure p in the gas cell, Γ_0 is the count rate at $p = 0$, σ is the total C_{60}^- destruction cross section to be determined, l is the length of the gas cell (4 cm), and k_B is Boltzmann’s constant. The temperature T is 300 K.

In order to determine the absolute cross section for the formation of a specific daughter ion such as C_{59}^- , we distribute the total cross section σ according to the corresponding number of product ions $N_i(p)$ relative to the number of intact parent ions $N_{par}(p)$ detected in the same spectrum:

$$\sigma_i = \sigma \frac{N_i(p)}{N_{par}(p)(e^{p\sigma l/k_B T} - 1)}, \quad (2)$$

where $N_{par}(p)(e^{p\sigma l/k_B T} - 1)$ corresponds to the total number of parent ions destroyed as this spectrum was recorded.

2.2. Calculations

Classical molecular dynamics simulations of collisions between C_{60} and He were carried out using the LAMMPS software package [33]. We used the reactive Tersoff potential [34, 35] to describe the bonds between C atoms and the Ziegler-Biersack-Littmark (ZBL) potential [36] for the He- C_{60} interaction. For each collision energy 10,000 randomly oriented trajectories were simulated (with random orientations of the C_{60} molecule) and followed for 500 fs with a time step of 5×10^{-18} s. One frame from a trajectory leading the formation of the $He@C_{59}^-$ reaction product is shown in Figure 1. The full video of this trajectory is available in the electronic version of this article.

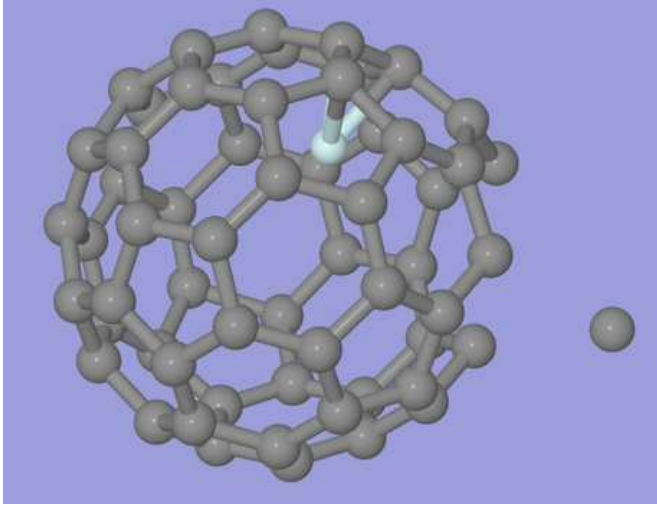


Figure 1: Image from a video of a MD trajectory leading to He@C_{59}^- . The C atom (black) at the right of the frame has been knocked out by the He atom (blue), which has been captured by the C_{59} cage. The full video is available in the electronic version of this article.

Charge	C_{60}	$ho\text{-C}_{59}$	$pn\text{-C}_{59}$
-1	2.59	3.56	3.37
0	7.50	6.69	6.93

Table 1: Electron binding energies (in eV) for fullerene anions and neutrals calculated with DFT at the B3LYP/6-31+G(d) level. See text for isomer naming convention.

Density Functional Theory (DFT) was used to calculate electron detachment and dissociation energies of C_{60}^- and C_{59}^- . These calculations were performed using Gaussian09 [37] at the B3LYP/6-31+G(d) level. Following the removal of a single carbon atom from C_{60} , there are two closed-cage structures of C_{59} to which the system may relax. These differ in the bonding between the three C atoms which were adjacent to the knocked out C; the naming here is adopted from Ref. [8]. The $ho\text{-C}_{59}^-$ isomer, in which the cage-closing leads to the formation of a hexagonal (h) and an octagonal (o) ring at the vacancy site, is 1 eV lower in energy than $pn\text{-C}_{59}^-$, where a pentagonal (p) and a nonagonal (n) ring are formed. For C_{58}^- , the lowest energy neutral isomer from Ref. [38], labeled $\text{C}_{3v}\text{-C}_{58}$, was used as a starting point for the calculations.

3. Results

3.1. Stability of C_{59}^-

Electron binding energies for both neutral and anionic C_{60} and C_{59} (both ho and pn isomers) are presented in Table 1. The present value for the electron affinity of C_{60} , 2.59 eV, is close to measured values (*e.g.* 2.664 eV [29]). Because of the dangling bonds, the electron affinity for both isomers of C_{59} are much higher at 3.56 eV for $ho\text{-C}_{59}$ and 3.37 eV for $pn\text{-C}_{59}$.

DFT-calculated dissociation energies for the main decay channels are given in Table 2. Our value for the $\text{C}_{60}^- \rightarrow$

Charge	$\text{C}_{60}^- \rightarrow \text{C}_{59}^- + \text{C}$	$\text{C}_{60}^- \rightarrow \text{C}_{58}^- + \text{C}_2$	$\text{C}_{59}^- \rightarrow \text{C}_{58}^- + \text{C}$
-1	11.6	10.1	4.54
0	12.6		
+1	11.8		

Table 2: Dissociation energies (in eV) for lowest energy isomers of C_{59} and C_{58} , $ho\text{-C}_{59}$ and $\text{C}_{3v}\text{-C}_{58}$, in various charge states calculated with DFT at the B3LYP/6-31+G(d) level.

$\text{C}_{58}^- + \text{C}_2$ dissociation energy of 10.1 eV is similar to the 10–11 eV measured for neutral and cationic C_{60} [27, 26]. The dissociation energy for $\text{C}_{60}^- \rightarrow \text{C}_{59}^- + \text{C}$, which we calculate for anionic, neutral and cationic species, is around 12 eV which is significantly higher than for C_2 -loss from C_{60} in all cases and in agreement with previous calculations (for neutrals and cations [8]). The dissociation energy calculated, however, does not consider any energy barrier between the initial and final states. Given that C_{59} is almost never observed in fullerene fragmentation experiments, even when employing excitation energies far in excess of all dissociation energies, it is possible that much higher barriers are present for $\text{C}_{60}^- \rightarrow \text{C}_{59}^- + \text{C}$ than for $\text{C}_{60}^- \rightarrow \text{C}_{58}^- + \text{C}_2$ fragmentation processes. In contrast to the dissociation energy, the threshold displacement energy T_d reflects the barriers for the $\text{C}_{60}^- \rightarrow \text{C}_{59}^- + \text{C}$ process.

Our calculated dissociation energy for $\text{C}_{59}^- \rightarrow \text{C}_{58}^- + \text{C}$ is rather low at 4.54 eV and close to the previously calculated 5.4 eV for C_{59}^+ [8]. This is also likely to contribute to the low observed yield of C_{59} in experiments – the products are fragile and may rather easily undergo delayed fragmentation processes. Internal energies upwards of 40 eV are known to be required to observe C_2 -loss from fullerenes on microsecond timescales [38]. Formation of C_{59} in a statistical process would involve similar if not higher internal energies, most of which would remain with the C_{59} leading to further C-loss. For non-statistical knockout fragmentation, however, much of the collision energy is carried away by the knocked out C atom, leaving colder C_{59} . In the case of C_{59}^- anions, the dissociation energy is comparable to the electron binding energy, and these decay channels can be expected to compete.

3.2. Total destruction cross sections

Experimental total destruction cross sections for $\text{C}_{60}^- + \text{He}$ collisions are determined by measuring the attenuation of the C_{60}^- beam as a function of He target density [31] and the results are shown for a range of different center-of-mass collision energies in Figure 2. Also shown in Figure 2 are the single carbon knockout cross section from our MD simulations. These simulations indicate that knockout only gives a small contribution to the total C_{60}^- destruction cross section. Furthermore, the simulations do not include secondary fragmentation or electron emission processes and should thus be considered upper limits for C_{59}^- formation.

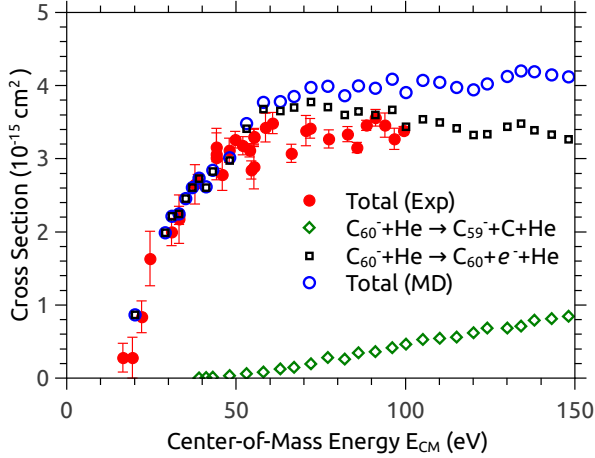


Figure 2: Absolute total destruction cross section for C_{60}^- in collisions with He determined from beam attenuation measurements (filled circles). Carbon knockout cross sections ($C_{60}^- + \text{He} \rightarrow C_{59}^- + \text{C} + \text{He}$) from MD simulations, electron emission cross sections ($C_{60}^- + \text{He} \rightarrow C_{60} + e^- + \text{He}$) from the statistical model described in the text, and the sum of these two channels (open diamonds, squares, and circles, respectively).

Our MD simulations model only the nuclear scattering part of the He- C_{60} interaction and does not include the scattering of the He atom on the electrons in C_{60} or delayed decay processes such as unimolecular dissociation (*i.e.* statistical fragmentation) or thermionic electron emission. Depending on the kinetic energy of the incident C_{60}^- ions, product ions travel for 10–40 μs between the gas cell and the mass analyzing system [30, 31], giving ample time for such delayed processes to occur. Nevertheless, we can use the fullerene excitation energies from simulations to reproduce the measured total C_{60}^- destruction cross section, which is presumably dominated by electron loss, using a statistical model. All parameters used in this model are taken from the present DFT calculation (Tables 1 and 2) or from the literature as detailed below. None of these parameters are adjusted to obtain agreement with experiment. The same model will also be used in Section 3.4 to estimate the fraction of C_{59}^- that is produced sufficiently cold to survive the flight from the gas cell to the end of the deflection field in the kinetic-energy-per-charge analyzer without losing the electron.

Here, we will first consider the survival probability of collisionally excited C_{60}^- ions flying through the energy analyzer. First, the excitation energy deposited in the system is extracted from the MD simulations, taking the nuclear scattering on 60 carbon atoms into account. To this we add the internal energy of C_{60}^- before the collision, which is taken to be 0.44 eV for ~ 300 K C_{60} as calculated by Yoo *et al.* [39]. Finally, we add a small energy contribution from electronic stopping obtained by scaling the results by Schlathölter *et al.* [40] to the collision velocity in the present experiment. Adding these three contributions, we arrive at a total internal energy E_{int} for each individual

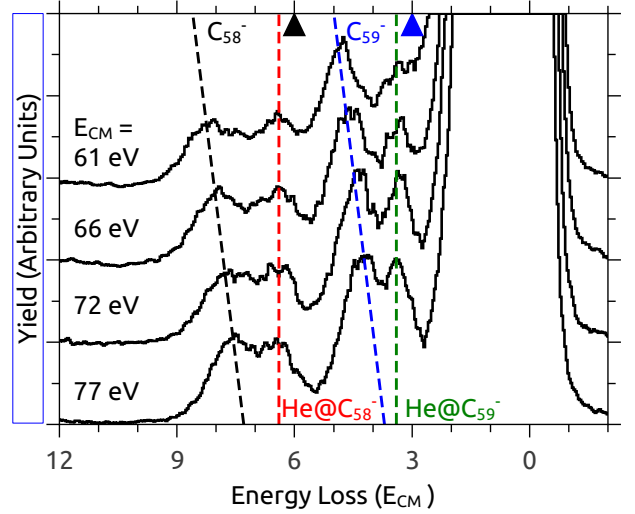


Figure 3: Negatively charged product distributions following $C_{60}^- + \text{He}$ collisions recorded at several values of E_{CM} . The dashed lines are to guide the eye. The measured energy loss (the difference in kinetic energy between the incident C_{60}^- ion and the fragment anion is due to the combination of the change in mass and the energy transfer to the internal degrees of freedom of the molecular system and is given on the lower horizontal scale in units of E_{CM} . The expected kinetic energies of C_{59}^- (blue) and C_{58}^- (black) fragments with the same velocity as incident C_{60}^- are indicated with arrowheads on the upper horizontal axis.

trajectory in the MD-simulation, an internal temperature $T[\text{K}] = 1000 + (E_{\text{int}}[\text{eV}] - 7.4)/C$ [41]. The effective temperature is then $T_{\text{eff}} = T - E_b/2C$, where $C = 0.138$ K/eV is the heat capacity of C_{60} [41], and $E_b = 2.664$ eV is the electron binding energy of C_{60}^- (the electron affinity of C_{60}) [29]. We calculate the survival probability for C_{60}^- ions as a function of their internal energy E_{int} by applying an Arrhenius expression for the electron detachment rate $k = \nu e^{-E_b/k_B T_{\text{eff}}}$ [32]. Here the pre-exponential factor ν is taken to be 10^{13} s^{-1} [42], and k_B is Boltzmann’s constant. This model gives a maximum internal energy of 16–17 eV for C_{60}^- to survive our experimental timescales of 10–40 μs , depending on the acceleration energy.

By combining the statistical model for electron loss and the MD simulations for knockout, we obtain the total C_{60}^- destruction cross section (knockout plus electron loss) shown in Figure 2. The agreement with the corresponding measured quantity is satisfactory, validating our computational approach, and indicating that electron emission is indeed the dominant C_{60}^- destruction mechanism in this energy range. In particular we see an onset of the experimental total C_{60}^- destruction cross section around 16 eV which is consistent with the results from the statistical model - with center-of-mass collision energies below 16 eV, the system cannot be sufficiently heated to emit an electron on the experimental timescale.

3.3. Product distributions

In Figure 3 we show distributions of negatively charged reaction products of $C_{60}^- + \text{He}$ collisions for center-of-mass

collision energies ranging from $E_{CM} = 61$ eV to $E_{CM} = 77$ eV, which corresponds to kinetic energies of 11–14 keV keV for the incident C_{60}^- ions in the laboratory reference frame. The collision products contributing to the energy spectra in Figure 3 are those which are sufficiently cold to retain their negative charge through the analyzing system after the gas cell. The spectra are measured under single-collision conditions as has been confirmed by measuring the C_{60}^- beam attenuation as a function of pressure in the gas cell. The distributions are plotted on an $E_{loss} = E_{parent} - E_{product}$ scale – the difference in kinetic energy of the parent ion C_{60}^- and the product ion – in units of the center-of-mass collision energy E_{CM} . The measured kinetic energy loss is due not only to the difference in mass between the incident C_{60}^- ion and the product anion but also to the energy transferred to the internal degrees of freedom of the molecular system. Capture of the He atom by the fullerene cage also reduces the kinetic energy. The energy loss due only to mass loss from C_{60}^- without energy transfer would be $3N_{loss}^C \times E_{CM}$ where N_{loss}^C is the number of C atoms lost. The expected positions of C_{59}^- and C_{58}^- fragments with the same velocity as the incident C_{60}^- ions would thus be $E_{loss} = 3 \times E_{CM}$ and $E_{loss} = 6 \times E_{CM}$, respectively, and are indicated with arrowheads on the upper axis of Figure 3.

The energy spectra are dominated by intact C_{60}^- ions at $E_{loss} = 0$. Four daughter anion peaks are observed: two just below the expected C_{59}^- energy ($E_{loss} = 3 \times E_{CM}$), and two just below the expected C_{58}^- energy ($E_{loss} = 6 \times E_{CM}$). Based on comparisons with our MD simulations (*vide infra*), we assign in both cases the higher energy peaks to endohedral complexes. The daughter ion peak with the highest kinetic energy (smallest energy loss) is the first observation of an endohedral defect fullerene complex with an odd number of C atoms, namely $He@C_{59}^-$.

The observed C_{58}^- and $He@C_{58}^-$ products are most likely due to secondary losses of loosely bound C atoms from C_{59}^- and $He@C_{59}^-$, respectively. We have calculated the $C_{59}^- \rightarrow C_{58}^- + C$ dissociation energy to be 4.54 eV (see Table 2), and that for the endohedral complex is likely comparable. Direct statistical dissociation $C_{60}^- \rightarrow C_{58}^- + C_2$ has a dissociation energy of 10.1 eV according to our calculations and is not competitive with electron emission (2.664 eV [29]) and thus should not contribute significantly to the negative product spectrum.

As can be seen in Figure 3, the peaks in the product distributions assigned to endohedrals remain roughly at the same E_{loss} values, while the C_{59}^- and C_{58}^- peaks shift to greater E_{loss} values with decreasing E_{CM} . In the top panel of Figure 4, we compare the measured and simulated mean energy loss for the observed product ions as a function of E_{CM} . For the experimental data, these values are extracted by fitting Gaussian peak shapes to each of the four daughter ions; two Gaussians are used for the tail of the parent C_{60}^- peak. The peaks assigned to endohedral complexes are shifted by between 0.25 to 0.5 units of E_{CM} relative to the expected E_{loss} values for C_{59}^- and C_{58}^-

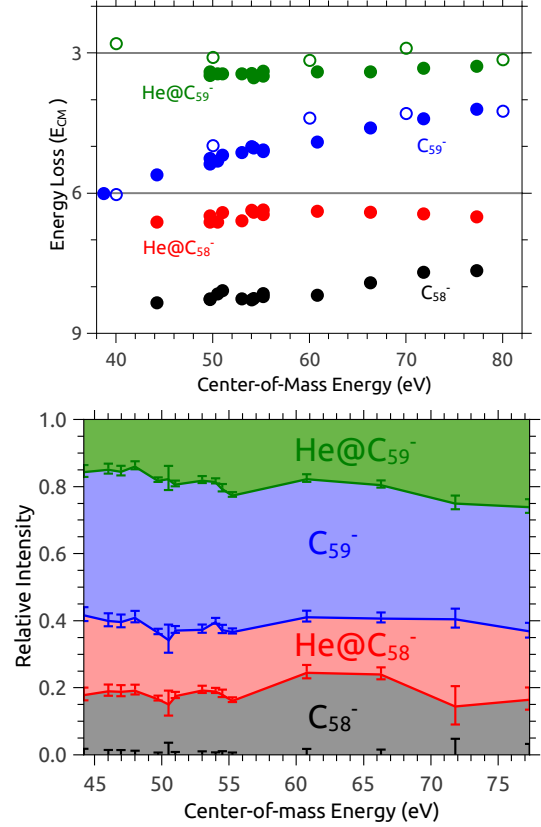


Figure 4: Top: Mean energy losses of reaction products in units of E_{CM} ; filled symbols: experiment, open symbols: MD simulations. The uncertainties in the mean position are smaller than the symbols. Bottom: Stacked area plot showing the relative intensities of the product peaks as a function of E_{CM} .

with the same velocity as the incident C_{60}^- ion at $3 \times E_{CM}$ and $6 \times E_{CM}$, respectively, which are indicated by horizontal lines in the upper panel of Figure 4. This is different from the situation when atoms like He are captured by intact C_{60} , where the increase in mass induces a well-defined energy loss equal to E_{CM} [43]. For $He@C_{59}^-$ formation, the knocked out carbon atom carries away some energy and energy losses smaller than E_{CM} are therefore possible. Knockout collisions without capture giving C_{59}^- and C_{58}^- have a broader range of possible energy transfers and are thus shifted by larger energies on average. Mean energy losses from our MD simulations are in good agreement with the experimental values for $He@C_{59}^-$ and C_{59}^- . It is important to note that the MD simulations reproduce the different dependencies of the center-of-mass collision energy for both these fragments – the energy loss increases with decreasing collision energy for the C_{59}^- fragment while the energy loss of the endohedral complex $He@C_{59}^-$ remains close to constant in both the experiment and in the simulations.

The energy shifts of the experimentally observed $He@C_{58}^-$ and C_{58}^- products relative to the expected energy of C_{58}^- are similar to those of C_{59}^- and $He@C_{59}^-$, respectively. This

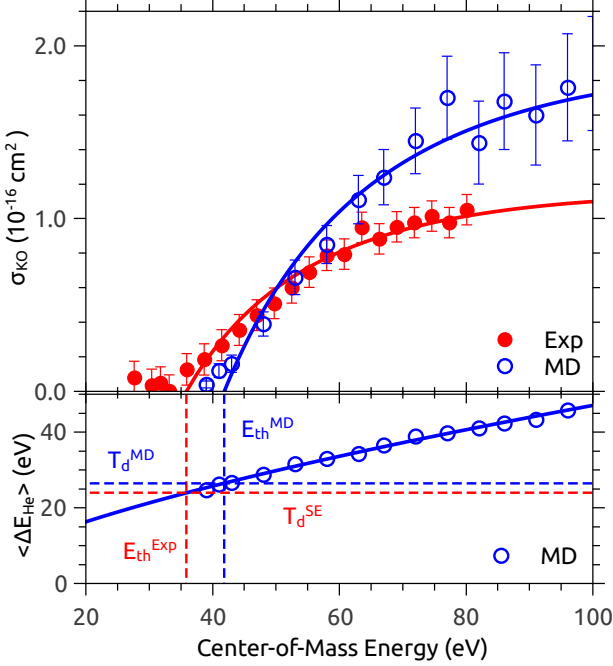


Figure 5: Above: experimental and simulated cross sections for detection of daughter anions arising from non-statistical fragmentation in $C_{60}^- + He$ collisions. For the simulations, C_{59}^- daughters predicted to be lost to electron emission by our statistical model are excluded from the cross section (*cf.* Figure 5). The solid lines are fits to Eq. (3) which gives the threshold energy E_{th} . Below: MD-simulated mean He-C energy transfers $\langle \Delta E_{He} \rangle$ in collisions leading to C_{59}^- fragments cold enough to survive the experiment. The solid line is a power law fit; dashed lines illustrate the determination of the threshold displacement energy T_d .

is consistent with our view that these products originate from $C_{59}^- \rightarrow C_{58}^- + C$ as a second step after knockout. Our MD simulations do not include statistical fragmentation processes such as $C_{59}^- \rightarrow C_{58}^- + C$ and we are thus unable to compare simulation with experiment in this case.

In the bottom panel of Figure 4, one can see that the relative intensities of the four anion fragment peaks (again extracted using Gaussian fits) vary little as a function of the collision energy down to 45 eV, beyond which we cannot resolve $He@C_{59}^-$ from the tail of the C_{60}^- peak. This supports our interpretation that all four products arise from a common mechanism with a single threshold energy.

3.4. Threshold displacement energy

As discussed above, the four different reaction channels leading to the production of $He@C_{59}^-$, C_{59}^- , $He@C_{58}^-$, or C_{58}^- fragments are all non-statistical in nature and can be considered to be due to a common mechanism. Accordingly, we deduce the total absolute cross section for non-statistical fragmentation from our mass spectra by summing the intensities of all four anion fragment peaks and relating this sum to the C_{60}^- total destruction cross section as described in Section 2.1. The resulting experimental cross section for $C_{60}^- + He$ collisions yielding negatively charged fragments is given in the upper panel of Figure 5.

Also included in Figure 5 are results from our MD simulations combined with our statistical model for delayed electron emission from C_{59}^- products. In the upper panel we give the cross section for single carbon knockout and in the lower panel the average energy transfer to the molecular system $\langle \Delta E_{He} \rangle$ in collisions leading to C knockout. Included in both of these quantities are only those trajectories which leave the resulting C_{59}^- sufficiently cold to survive the timescale of our experiment. To calculate the survival probability of C_{59}^- , we first determine the internal energy of C_{59}^- at the end of each MD trajectory. The heat capacity for C_{59}^- is found by scaling that of C_{60}^- by the number of degrees of freedom, and we use a value of 3.56 eV for the electron binding energy (Table 1). Due to the higher electron binding energy of C_{59}^- compared to C_{60}^- , our statistical model gives a higher internal energy cutoff of 24-25 eV for C_{59}^- to survive until detection in the experiment. The effects of these considerations are negligible for $E_{CM} < 60$ eV but there are significant corrections for higher energies. For comparison to experiment, we do not need to consider the competitive $C_{59}^- \rightarrow C_{58}^- + C$ channel, as C_{58}^- is included in our total non-statistical product cross section.

The experimental and simulated cross sections are qualitatively similar, albeit with an offset in the observed threshold energy for knockout. Such an offset has been observed previously in comparison between experimental and simulated knockout cross sections [17], and may be due to the approximate, classical nature of the Tersoff potential used to model the C-C bonds. To determine the threshold energy for carbon knockout, we model the experimental and MD cross section assuming that the primary process is an elastic binary collision between a He projectile with kinetic energy equal to the He- C_{60}^- center-of-mass E_{CM} and a free C atom at rest. This is justified in that the knockout process happens on an ultrafast timescale on which the remaining 59 C atoms are standing still. For such collisions, Chen *et al.* [44] give the following expression, based on Lindhard scattering theory [45], for the cross section σ_{KO} leading to energy transfer above a given fixed value (here the displacement energy T_d):

$$\sigma_{KO} = \frac{A/E_{CM}}{\pi^2 \arccos^{-2}(\sqrt{E_{th}/E_{CM}}) - 4}, \quad (3)$$

where E_{th} is the minimum center-of-mass energy (for the He- C_{60} system) required to transfer T_d . We take A and E_{th} as fit parameters, yielding $E_{th}^{exp} = 35.8 \pm 0.5$ eV and $E_{th}^{MD} = 41.8 \pm 1.5$ eV. As seen in Figure 5, this simple model accurately reproduces both the experimental and MD cross sections above E_{th} . There is some (barely significant) deviation close to threshold, which probably due to the fact that T_d is not single-valued, but rather varies somewhat with respect to the angles between the imparted momentum and the molecular bonds [13, 14], as well as with the stretching of the bonds due to molecular vibrations [15].

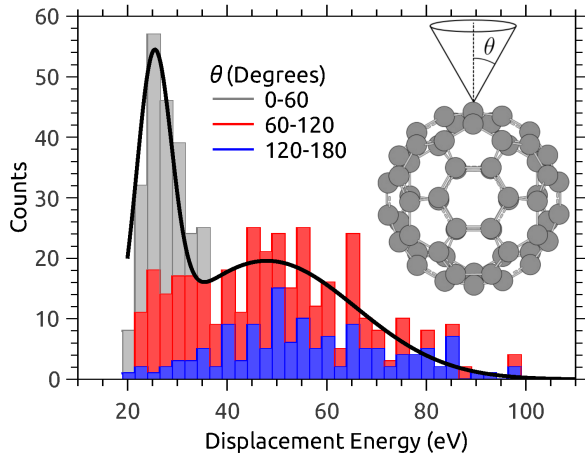


Figure 6: Histogram of displacement energies from projectile-free MD simulations. The solid line is a fit to the sum of two Gaussians describing a bimodal distribution.

The threshold energy E_{th} is projectile dependent [12]; to obtain the intrinsic threshold displacement energy T_d we need the energy transferred from the projectile (He) to the target at threshold, which we extract from our MD simulations. From a power-law fit to $\langle \Delta E_{He} \rangle = c \times E_{CM}^P$ we obtain the mean energy transfer at the experimental knockout threshold $E_{CM} = E_{th}^{exp}$. This is our semi-empirical value for the $C_{60} \rightarrow C_{59} + C$ threshold displacement energy, $T_d^{SE} = 24.1 \pm 0.5$ eV. The uncertainty given here is calculated from the uncertainty in the power-law fit parameters c and P , and E_{th}^{exp} . Our semi-empirical value of T_d is much higher than generally assumed previously for fullerenes (around 15 eV [18, 19, 20, 2]), and is similar to those measured for the planar sp^2 -hybridized carbon systems graphene (23.6 eV [15, 16]) and PAHs (23.3 ± 0.3 eV [17]).

As our MD simulations give a somewhat higher threshold energy than the measurements we find a correspondingly higher threshold displacement energy $T_d^{MD} = 26.5 \pm 0.8$ eV, which is slightly lower than previous simulation-based results [13].

We have also performed projectile-free MD simulations, where an individual C atom is simply assigned a certain velocity at a given angle relative to the axis connecting the atom and the center of the fullerene cage. The minimum energy at which the atom is removed is the displacement energy for that angle. A histogram of these results is shown in Figure 6, which shows a clear bimodal distribution. A fit to the sum of two Gaussians gives the centroid of the low-energy mode as 25.3 ± 0.4 eV with a width of 7 ± 1 eV. This is consistent with our result for the full simulations including the He projectile. Trajectories contributing to the high-energy mode of the histogram in Figure 6 would presumably be left with internal energies too high to survive the experiment.

Notably, most of the trajectories contributing to the low-energy mode are at angles pointed outwards from the

center of the fullerene cage. This helps explain the surprisingly high abundance of endohedral complexes in our experiments. The He projectile must first penetrate the cage prior to the knockout collision, in which a large fraction of its energy is transferred to the knocked out C atom, leaving the backscattered He with insufficient energy to escape the (now defective) cage.

4. Conclusions

This is, to our knowledge, the first determination of a threshold displacement energy for free fullerenes or for any type of fullerene based material. This intrinsic material property is a key parameter for modeling radiation damage in many contexts, for example during electron microscopy imaging [15] or gas-phase reactions in the interstellar medium [12]. Finally, the surprising observation of the endohedral defect fullerene complex $He@C_{59}^-$ is a remarkable testament to the intriguing complexity of fullerene reactions, which continue to fascinate more than 30 years after their discovery.

5. Acknowledgments

This work was performed at the Swedish National Infrastructure, DESIREE (Swedish Research Council Contract No. 2017-00621). It was further supported by the Swedish Research Council (grant numbers 2014-4501, 2015-04990, 2016-03675, 2016-04181, 2016-06625). See Supplemental Material for videos of selected MD simulations.

References

- [1] A. J. McKenna, T. Trevethan, C. D. Latham, P. J. Young, M. I. Heggie, Threshold displacement energy and damage function in graphite from molecular dynamics, *Carbon* 99 (2016) 71–78.
- [2] H. Zettergren, et al., Formations of Dumbbell C_{118} and C_{119} inside Clust, *Phys. Rev. Lett.* 110 (2013) 185501.
- [3] M. H. Stockett, et al., Nonstatistical fragmentation of large molecules, *Phys. Rev. A* 89 (2014) 032701.
- [4] F. Banhart, J. Kotakoski, A. V. Krasheninnikov, Structural defects in graphene, *ACS Nano* 5 (1) (2010) 26–41.
- [5] A. V. Krasheninnikov, K. Nordlund, Ion and electron irradiation-induced effects in nanostructured materials, *J. Appl. Phys.* 107 (7) (2010) 3.
- [6] J. Kotakoski, F. R. Eder, J. C. Meyer, Atomic structure and energetics of large vacancies in graphene, *Phys. Rev. B* 89 (20) (2014) 201406.
- [7] F. Seitz, et al., Ions colliding with clusters of fullerenes – Decay pathways, *J. Chem. Phys.* 139 (3) (2013) 034309.
- [8] Y. Wang, et al., Formation dynamics of fullerene dimers C_{118}^+ , C_{119}^+ , and C_{120}^+ , *Phys. Rev. A* 89 (2014) 062708.
- [9] R. F. Egerton, M. Takeuchi, Radiation damage to fullerite (C_{60}) in the transmission electron microscope, *Appl. Phys. Lett.* 75 (13) (1999) 1884–1886.
- [10] O. P. Dmytrenko, et al., Dose dependences of the optical properties of full, *Thin Solid Films* 495 (1) (2006) 365 – 367.
- [11] E. R. Micelotta, A. P. Jones, A. G. G. M. Tielens, Polycyclic aromatic hydrocarbon processing in interstellar shocks, *Astron. Astrophys.* 510 (2010) A36.
- [12] J. Postma, R. Hoekstra, A. G. G. M. Tielens, T. Schlathölter, A Molecular Dynamics study on slow ion interactions with the Polycyclic, *Astrophys. J.* 783 (1) (2014) 61.

- [13] F. Z. Cui, H. D. Li, X. Y. Huang, Atomistic simulation of radiation damage to C_{60} , *Phys. Rev. B* 49 (14) (1994) 9962.
- [14] M. Gatchell, H. Zettergren, Knockout driven reactions in complex molecules and their clusters, *J. Phys. B* 49 (16) (2016) 162001.
- [15] J. C. Meyer, et al., Accurate measurement of electron beam induced displacement cross sections for collisions of deuterium with Fullerenes, *Phys. Rev. Lett.* 108 (2012) 196102.
- [16] J. C. Meyer, et al., Erratum: Accurate measurement of electron beam induced displacement cross sections for collisions of deuterium with Fullerenes, *Phys. Rev. Lett.* 110 (2013) 239902.
- [17] M. H. Stockett, M. Gatchell, T. Chen, N. de Ruette, L. Giacomozzi, M. Wolf, H. T. Schmidt, H. Zettergren, H. Cederquist, Threshold energies for single-carbon knockout from polycyclic aromatic hydrocarbons, *J. Phys. Chem. Lett.* 6 (22) (2015) 4504–4509.
- [18] T. Füller, F. Banhart, In situ observation of the formation and stability of single fullerene molecules under electron irradiation, *Chem Phys Lett* 254 (5-6) (1996) 372–378.
- [19] E. Parilis, Atomic collisions with accelerated fullerenes, *Nucl. Instrum. Methods Phys. Res., Sect. B* 88 (1-2) (1994) 21–24.
- [20] M. C. Larsen, P. Hvelplund, M. O. Larsson, H. Shen, Fragmentation of fast positive and negative C_{60} ions in collisions with rare gas atoms, *Eur. Phys. J. D* 5 (2) (1999) 283–289.
- [21] T. Weiske, D. K. Böhme, J. Hrušák, W. Krätschmer, H. Schwarz, Endohedral cluster compounds: Inclusion of helium within C_{60}^+ and C_{70}^+ through collision experiments, *Angew. Chem. Int. Ed.* 30 (7) (1991) 884–886.
- [22] H. Sprang, A. Mahlkow, E. E. B. Campbell, Collisional energy dependence of the capture by internally excited C_{60} anions, *Chem. Phys. Lett.* 227 (1) (1994) 91 – 97.
- [23] E. E. B. Campbell, R. Ehlich, G. Heusler, O. Knospe, H. Sprang, Capture dynamics in collisions between fullerene ions and rare gas atoms, *Chem. Phys.* 239 (1) (1998) 299–308.
- [24] K. Komatsu, M. Murata, Y. Murata, Encapsulation of molecular hydrogen in fullerene C_{60} by organic synthesis, *Science* 307 (5707) (2005) 238–240.
- [25] K. Kurotobi, Y. Murata, A single molecule of water encapsulated in fullerene C_{60} , *Science* 333 (6042) (2011) 613–616.
- [26] S. Tomita, J. U. Andersen, C. Gottrup, P. Hvelplund, U. V. Pedersen, Dissociation Energy for C_2 Loss from Fullerene Cations in a Storage Ring, *Phys. Rev. Lett.* 87 (2001) 073401.
- [27] S. Tomita, J. U. Andersen, K. Hansen, P. Hvelplund, Stability of buckminsterfullerene, C_{60} , *Chem. Phys. Lett.* 382 (1) (2003) 120 – 125.
- [28] M. Gatchell, et al., Non-statistical fragmentation of PAHs and fullerenes in collisions with atoms, *Int. J. Mass Spectrom.* 365–366 (0) (2014) 260–265.
- [29] K. Støchkel, J. U. Andersen, Photo excitation and laser detachment of C_{60}^- anions in a storage ring, *J. Chem. Phys.* 139 (16) (2013) 164304.
- [30] M. H. Stockett, et al., Fragmentation of anthracene $C_{14}H_{10}$, acridine $C_{13}H_9N$ and phenazine $C_{12}H_8N_2$ ions in collisions with atoms, *Phys. Chem. Chem. Phys.* 16 (2014) 21980–21987.
- [31] N. de Ruette, M. Wolf, L. Giacomozzi, J. D. Alexander, M. Gatchell, M. H. Stockett, N. Haag, H. Zettergren, H. T. Schmidt, H. Cederquist, DESIREE electrospray ion source test bench and setup for collision induced dissociation experiments, *Rev. Sci. Instrum.* 89 (7) (2018) 075102. ,
- [32] S. Tomita, P. Hvelplund, S. B. Nielsen, T. Muramoto, C_{59} -ion formation in high-energy collisions between cold C_{60}^- and noble gases, *Phys. Rev. A* 65 (2002) 043201.
- [33] S. Plimpton, Fast parallel algorithms for short-range molecular dynamics, *J. Comput. Phys.* 117 (1) (1995) 1–19.
- [34] J. Tersoff, New empirical approach for the structure and energy of covalent systems, *Phys. Rev. B* 37 (1988) 6991–7000.
- [35] J. Tersoff, Modeling solid-state chemistry: Interatomic potentials for multicomponent systems, *Phys. Rev. B* 39 (1989) 5566–5568.
- [36] J. F. Ziegler, J. P. Biersack, U. Littmark, *in* The Stopping and Range of Ions in Matter, Pergamon, New York, 1985.
- [37] M. J. Frisch, et al., Gaussian 09, Revision D.01 (2009).
- [38] L. Chen, S. Martin, J. Bernard, R. Brédy, Direct Measurement of Internal Energy of Fragmented C_{60} , *Phys. Rev. Lett.* 98 (2007) 193401.
- [39] R. K. Yoo, B. Ruscic, J. Berkowitz, Vacuum ultraviolet photoionization mass spectrometric study of C_{60} , *J. Chem. Phys.* 96 (2) (1992) 911–918.
- [40] T. Schlathöler, O. Hadjar, R. Hoekstra, R. Morgenstern, Strong Velocity-Dependent Effects for Collisions of deuterium with Fullerenes, *Phys. Rev. Lett.* 82 (1999) 73–76.
- [41] J. U. Andersen, C. Gottrup, K. Hansen, P. Hvelplund, M. O. Larsson, Radiative cooling of fullerene anions in a storage ring, *Eur. Phys. J. D* 17 (2) (2001) 189–204.
- [42] J. U. Andersen, E. Bonderup, Classical dielectric models of fullerenes and estimation of heat radiation, *Eur. Phys. J. D* 11 (3) (2000) 413–434.
- [43] K. A. Caldwell, D. E. Giblin, M. L. Gross, High-energy collisions of fullerene radical cations with target gases: capture cross sections, *J. Am. Chem. Soc.* 114 (10) (1992) 3743–3756.
- [44] T. Chen, et al., Absolute fragmentation cross sections in atom-molecule collisions, *J. Chem. Phys.* 140 (22) (2014) 224300.
- [45] J. Lindhard, V. Nielsen, M. Scharff, Cross sections for ion-atom collisions in solids, *Mat.-Fys. Medd. K. Dan. Vidensk. Selsk* 36 (1968) 10.